Biol Cybern (2009) 100:371–383
DOI 10.1007/s00422-009-0308-7

ORIGINAL PAPER

Biological Cybernetics

Two-point heterogeneous connections in a continuum neural field model

C. A. Brackley · M. S. Turner

Received: 18 November 2008 / Accepted: 22 March 2009 / Published online: 7 April 2009

Abstract We examine a novel heterogeneous connection scheme in a 1D continuum neural field model. Multiple two-point connections are added to a local connection function in order to model the "patchy" connections seen in, for example visual cortex. We use a numerical approach to solve the equations, choosing the locations of the two-point connections stochastically. We observe self-sustained persistent fluctuations of activity which can be classified into two types (one of which is similar to that seen in network models of discrete excitable neurons, the other being particular to this model). We study the effect of parameters such as system size and the range, number and strength of connections, on the probability that a particular realisation of the connections is able to exhibit persistent fluctuations.

Keywords Neural field model · Patchy connections · Persistent fluctuations

1 Introduction

Continuum neural field (CNF) models such as those proposed by Wilson and Cowan (1972) and Amari (1977) in the 1970s treat neural tissue as a continuous medium, and describe the electrical activity (usually defined as the mean membrane potential of a population of neurons) using scalar fields. Such models examine behaviour on the mesoscopic scale, bridging the gap between small networks of spiking neurons [e.g. as modelled by Hopfield (1982) or Brunel (2000), and realised experimentally with techniques such as calcium imaging (Cossart et al. 2003) or multi-electrode arrays (Segev et al. 2002)] and high-level measurements such as EEG and MEG (which have been extensively modelled, e.g. by Robinson et al. 2002). Experimental probes of this mesoscopic length scale include local field potential and voltage sensitive dye imaging techniques (Bao and Wu 2003; Wu et al. 1999). In the past CNF models have been used to study phenomena such as visual hallucinations (Ermentrout and Cowan 1979), spread of epileptiform activity at seizure onset (Ermentrout and McLeod 1993; Pinto and Ermentrout 2001) and working memory (Amari 1977). One such model describes the dynamics of the fields using the equations

$$\begin{aligned} \tau_u \frac{\partial u}{\partial t} + u(x,t) &= \int_\Gamma w(x,x') f(u(x',t)) \mathrm{d}x' - g v(x,t), \\ \tau_v \frac{\partial v}{\partial t} + v(x,t) &= f(u(x,t)). \end{aligned} \tag{1}$$

Here we examine a 1D system in which the scalar fields $u(x,t)$ and $v(x,t)$ represent the activity of populations of excitatory and inhibitory neurons, respectively.[1] Γ denotes the extent of the system (in analytical work this is usually extended to $\pm\infty$, whereas in numerical work it is common to examine a finite system with periodic boundaries). In this model the two populations exist in the same space, the excitatory population acting to increase the activity of its target cells, and the inhibitory population to decrease the activity of target cells. The strength of the inhibition is given by the constant g, and the response time of each population by the constants τ_u and τ_v. Biologically τ_u and τ_v represent the synaptic response time of the populations; in models of this sort it is conventional to project the synaptic dynamics

C. A. Brackley (✉) · M. S. Turner
Department of Physics, University of Warwick,
Coventry CV4 7AL, UK
e-mail: c.a.brackley@warwick.ac.uk

[1] In an alternative model of "linear feedback", the v field represents not only inhibitory cells but also other processes such as synaptic depression; the right hand side of the equation for $\partial v/\partial t$ is replaced $f(u) \to u$.

to a single response time.[2] For simplicity (to reduce the number of free parameters) we initially take $\tau_v = \tau_u$; we return to this simplification in a later section where we look at the effect of changing τ_v. The choice $\tau_u = 1$ sets the time units for the system. The function $f(u)$ gives the firing rate of cells with activity u. Experimentally, for a population of cells, this is found to be of sigmoid form; as is conventional in these models, we approximate f as a discontinuous step $f(u) = \Theta(u - \theta)$ where $\Theta(y) = 1$ for $y \geq 0$ and $\Theta(y) = 0$ otherwise. The firing threshold θ is assumed to be a constant in space and time. A recent review of CNF models (Coombes 2005) discusses some of the possible variations of the model and the solutions they support, whilst (Jirsa 2004) puts these models in the wider context of information processing by networks. As a continuum, or mean field level model, features such as axonal and dendritic tree structure are encapsulated within the connection function, and the need to described the irregular spiking of cells is removed by taking a "firing rate" approach; we also ignore finite axonal conduction speeds. Although some of these features have been included explicitly in CNF models by other authors [e.g. Hutt et al. 2003 examine the effect of finite axonal conduction velocity, (Bressloff 1996; Coombes et al. 2003) consider the effect of axonal and dendritic structure, and Brackley and Turner (2007) consider the effect of spatially and temporally varying threshold] here we study a simpler model in order that we can attribute observed novel behaviour solely to inhomogeneous connections; we discuss this further in the conclusions section.

The strength of synaptic connections from a point x' to a point x is given by the function $w(x, x')$. A common assumption in previous work is that the connectivity is both homogeneous and isotropic, and the connection function is a simple function of separation $w(x, x') = w(|x - x'|)$ (common choices including exponential or Gaussian shaped functions). There is some experimental justification for such forms, for example Hellwig (2000) studies pyramidal neurons in cat visual cortex and finds that probability of finding a connection between cells decrease with their separation, roughly as a Gaussian function. Other studies show additional longer ranged connections, for example Malach et al. (1994) and Buzás et al. (2001) have identified "patchy" connections. Figure 1 shows an image of a cell in visual cortex area V2 which has been stained with biocytin (allowing the axonal fibres to be seen). As well as a central halo near the stain injection point there are also patches where there is a high density of axonal fibres at more distant points. Malach et al. found that patches could have a width of up to approximately 0.3mm and could be up to 5mm from the injection point. It is also found that cells tend to make patchy connections to regions of the cortex which have a similar response to particular stimuli (e.g. to regions of similar orientation preference or ocular dominance), and that the axonal density within a patch decreases with distance from the injection site.

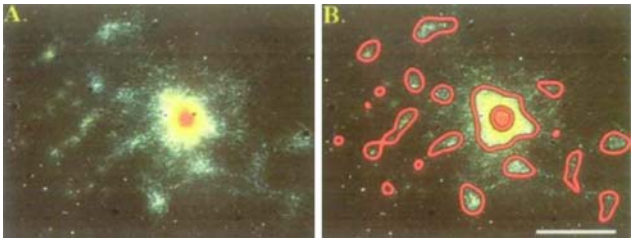

Fig. 1 Image **a** shows axons in visual cortex area V2 after injection with a stain. **b** shows the same image with axonal "patches" identified using a boundary detection algorithm. *Scale bar* is 1 mm. Reproduced from Malach et al. (1994) by permission of Oxford University Press

Previous attempts to include inhomogeneity in a field model include work by Bressloff (2001), who introduces a periodic inhomogeneity as a short length scale modulation of an otherwise homogeneous function. In Bressloff (2003) long-range horizontal connections were included in a 2D model. Also in Brackley and Turner (2009) long range connections with strength that varies stochastically (but continuously) in space are found to support persistent fluctuations of activity. In that slightly less general model, persistent activity resulted from having adjacent regions of the system in one of which there existed two stable steady states, with the other only supporting one. Due to non-linear feedback, activating the region with bistability resulted in persistent fluctuations at the boundary between the regions. Our strategy in this study is different in that we will model the "patchiness" of connections by introducing direct connections between individual points in our 1D system. Jirsa and Kelso (2000) use a similar idea in a slightly different model (which includes finite axonal propagation velocity), adding a single delta function connection between distant points to an otherwise homogeneous model. They examine pattern formation as a result of a uniform steady state becoming unstable, and study how this is effected by the distance over which the connection is formed; also a later paper (Qubbaj and Jirsa 2007) examines the effect of axonal conduction velocity on pattern formation. In contrast, in the current study we do not look at pattern formation, but focus on a parameter regime where the system can be switched from uniform quiescence to an active state.

We propose to include many long distance two-point connections with finite width. A similar idea is explored by Roxin et al. (2004) in a network model of discrete integrate and fire (IF) neurons. They create a small world network topology by taking an initially locally connected network, and randomly adding N unidirectional long ranged links. They study a regime where the IF neurons are excitable and travelling

[2] The form of this dependence of the population synaptic response time on measurable microscopic quantities such as the synaptic response of a single cell or the distance from synapse to soma is an open problem.

pulses of activity are possible. Introducing a small number of long range connections was shown to lead to a single pulse generating pairs of new pulses, leading to self-sustained persistent activity. Introducing more connections can lead to persistent activity *failure* as multiple pulses annihilate each other. Motivated by Roxin et al.'s work, in this work, we look for persistent activity in a continuum model (in the regime where travelling pulses are possible); i.e. we ask whether a phenomena seen at the level of a small network of cells can be seen in a continuum model at macroscopic length scales. We introduce two-point connections between stochastically selected points, which necessitates a numerical approach. We look at a finite system of length L and employ periodic boundary conditions.

In the next section we describe the heterogeneous connection function, before going on to look at persistent activity in Sect. 4. We include details of our numerical methods as an appendix at the end of the paper.

2 Heterogeneous connection functions

Since there is much evidence that locally the number of connections between cells decreases with distance, we treat the inhomogeneity as a small perturbation to a homogeneous function

$$w(x,x') = w_H(|x-x'|) + Aw_I(x,x'), \tag{2}$$

where w_H is the inhomogeneous function, A determines the magnitude of the heterogeneous connections, and $w_I(x,x') = w_l(|x-x'|)w_A(x,x')$, where w_l is a function of separation, introduced to provide an envelope determining the maximum range over which two-point connections can be made. For the homogeneous connections we choose a simple Gaussian

$$w_H(y) = \frac{1}{\sqrt{\pi}}\mathrm{e}^{-y^2}, \tag{3}$$

where the unit width of the function sets the length scale of the system, and the pre-factor ensures the function normalises to unity (setting the units of activity); i.e. $\int_{-\infty}^{\infty} w_H(y)dy = 1$. For the inhomogeneous envelope we choose a similarly shaped function with width l

$$w_l(y) = \mathcal{N}\mathrm{e}^{-y^2/l^2}. \tag{4}$$

We discuss the normalisation $\mathcal{N}$ in Sect. 3.

The heterogeneous connection function w_A contains N two-point connections. For consistency we assume connection "patches" to have the same shape as the local connections,giving rise to a sum over Gaussian peaks in the x,x' plane

$$w_A(x,x') = \sum_{n=1}^{N} \frac{1}{N}\exp\left(\frac{-(x-x_n)^2-(x'-x_n')^2}{d^2}\right), \tag{5}$$

where the N peaks have width d and amplitude $1/N$ and represent connections from start point x_n' to end point x_n. The choice of amplitude $1/N$ means that increasing the number of two-point connections preserves the total connection density (in contrast to Roxin et al. 2004 where they add *extra* connections). Physically this assumes that neural tissue contains a fixed number of synapses determined by A, and by changing N (or l) we are altering how these are distributed through the tissue. The width d represents the spatial extent of the branching of dendrites and axons (for simplicity we keep these the same, i.e. the width of the Gaussian peaks are the same in the x and x' directions). Although Malach et al.'s experimental work (see Malach et al. 1994; Fig. 1) suggests the "width" of a patchy connection is less than that of local connections, we choose $d = 1$ for simplicity; we re-examine the effect of this in the conclusion section. To construct a stochastic connection function we could choose the positions of the peaks $\{x_n, x_n'\}$ using a uniform random number generator, however, this could lead to several peaks lying on top of each other, introducing clusters of high-connection density. Whilst this may in itself provide interesting behaviour, in the first instance we seek to reduce such clustering. Instead of generating (pseudo-)random numbers, we use a sequence of (maximally avoiding) quasi-random numbers (see the Appendix; Press et al. 1992). Note that although each pair of coordinates x_n, x_n' represents a single unidirectional two-point connection, there can be multiple long range connections emanating from a single point.

Figure 2 shows a typical connection kernel w_A as a colour plot on the 2D x–x' plane for $N = 150$ two-point connections. Also shown is the full connection function $w(x,x')$ including the projection to $x' = 35$. Only the peaks in w_A which lie within a distance l of the diagonal $x = x'$ contribute to the full connection function. We note that there are two new quantities which describe the connections in our system; N/L^2 which gives the density of peaks in the x–x' plane, and Nl/L which approximates the total number of connections contributing to $w(x,x')$.

3 Solutions to the model

In order to compare with results for IF neurons (Roxin et al. 2004) we focus on the regime where travelling pulse solutions exist. As detailed in Coombes (2005) homogeneous CNF models can support travelling fronts and travelling pulses, depending the choice of parameters.

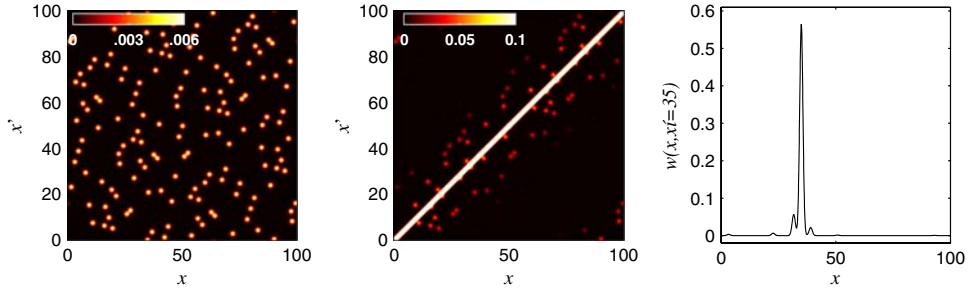

Fig. 2 *Left* colour plot showing the function $w_A(x, x')$ for a system of length $L = 100$ with $N = 150$ peaks. *Centre* colour plot showing the full connection function $w(x, x')$ with $l = 20$. *Right* plot of the same connection function at the (arbitrary) output location $x' = 35$. Note that although each connection peak in w_A connects two single points, this can lead to input to one point from multiple distant points

Travelling front solutions arise due to the fact that it is possible to arrange the system so that there are two stable steady states. Setting $A = 0$ to regain the homogeneous model, these steady states are found by setting $\partial_t u, \partial_t v = 0$ and $u(x, t) \to \bar{u}$ in Eq. (1), giving

$$\bar{u} = f(\bar{u}) \left[\int_{-\infty}^{\infty} w_H(|x - x'|) \mathrm{d}x' - g \right], \\ = f(\bar{u})[1 - g]. \tag{6}$$

From this we see that depending on the value of g there may be either two solutions (two stable steady states, $\bar{u}_1 = 0$ and $\bar{u}_2 = 1 - g$) or one solution (a single stable steady state $\bar{u}_1 = 0$); a full treatment is given in Coombes (2005). Travelling fronts are stable solutions in systems where there are two steady states; if one region of a system is initiated such that it resides in the upper steady state, and an adjacent region in the lower steady state, a front of activity will join the two, propagating with velocity depending on the threshold θ.

In the inhomogeneous case ($A \neq 0$) the upper steady state $\bar{u}_2$ is a function of x, and may or may not exist for all x. Proceeding in the same way, taking the steady state of Eq. (1) we get

$$\bar{u}(x) = f(\bar{u}(x))W(x), \tag{7}$$

where $\bar{u}$ is explicitly written as a function of x to reflect the inhomogeneous connections, and

$$W(x) = \int_{-\infty}^{\infty} \Big[w_H(|x - x'|) + A w_I(x, x') \Big] \mathrm{d}x' - g, \tag{8}$$

which describes the amplitude of connections into point x. We note that two solutions to (7) only exist if $W(x) \geq \theta$ (since the firing rate function f is a step at threshold θ). Anywhere where $W(x) \geq \theta$ an upper steady state exits locally (and the activity of this state is given by $W(x)$). At any point x where $W(x) < \theta$, there is only a single ($\bar{u} = 0$) steady state. If two stable steady states exist for all x, travelling front solutions are possible.

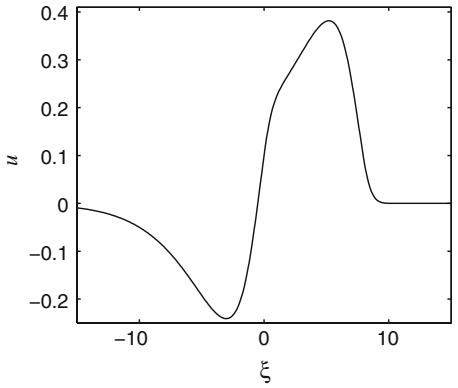

Fig. 3 *Plot* showing a travelling pulse in a homogeneous system ($A = 0$) in a frame of reference where it is stationary ($\xi = x - ct$). In the lab frame this would be travelling to the right with speed c. The width of the pulse Δ is defined as the length of the region in which activity is above threshold

In the $A = 0$ system travelling pulse solutions exist as a result of including the inhibitory feedback $v(x, t)$, which can provide a region of depressed activity in the wake of an exited region—see Fig. 3. A full treatment for a homogeneous ($A = 0$) system is given in Amari (1977) and Coombes (2005); there it is shown that the stability of travelling pulses depends on parameters g and θ, as well as τ_v which here we keep fixed—see Sect. 7. In a homogeneous system a choice of $g = 1$ and $\theta = 0.1$ gives stable pulses but not fronts (see Coombes 2005), so we use this throughout the rest of this study. To initialise a travelling pulse requires a localised region of increased (greater than threshold) activity; this can be achieved by injecting a transient localised external input to an otherwise quiescent ($u = 0$) system.

We now discuss the normalisation constant $\mathcal{N}$. Since $W(x)$ is an important quantity for determining what kind of solutions are possible in our system it would be useful to be able to

control this directly. With the choice $g = 1$ Eq. (8) becomes

$$W(x) = A\mathcal{N} \int_{-\infty}^{\infty} \mathrm{e}^{-\frac{(x-x')^2}{l^2}} \sum_{n=1}^{N} \frac{1}{N} \mathrm{e}^{\frac{-(x-x_n)^2-(x'-x'_n)^2}{d^2}} \mathrm{d}x' \qquad (9)$$

If we take the large N limit we can calculate the value of the integral in this equation. We approximate that the sum is over an infinite number of peaks which are evenly spaced on the x, x' plane, i.e.

$$\sum_{n=1}^{N} \to \frac{1}{\delta^2} \int_{-\infty}^{\infty} \int_{-\infty}^{\infty} \mathrm{d}x_n \mathrm{d}x'_n,$$

where δ is the linear separation of the peaks. For N peaks in an area L^2, $\delta = L/\sqrt{N}$. We thereby obtain the continuum limit

$$W(x) = \frac{A\mathcal{N}}{L^2} \int_{-\infty}^{\infty} \int_{-\infty}^{\infty} \int_{-\infty}^{\infty} \mathrm{d}x' \mathrm{d}x_n \mathrm{d}x'_n \times \mathrm{e}^{-\frac{(x-x')^2}{l^2} - \frac{(x-x_n)^2+(x'-x'_n)^2}{d^2}} \qquad (10)$$

which can be solved to give $W(x) = A\mathcal{N}d^2 l\pi^{3/2}/L^2$. Thus a normalisation

$$\mathcal{N} = \frac{L^2}{d^2 l\pi^{3/2}}, \qquad (11)$$

is useful, as in the large N limit $W(x) \approx A$; i.e. we can control the strength of connections into point x by varying a single parameter A. We expect interesting solutions when $W(x)$ is close to threshold so we examine $A \sim \theta$.

4 Persistent activity

We look for self-sustained persistent activity by initialising the system such that $u = 0$ for all x, and injecting two pulses which move away from each other in opposite directions (we discuss these initial conditions in the next section). In the homogeneous ($A = 0$) case the pulses will travel across the entire (periodic) system until they meet. When two oppositely travelling pulses meet, the depressed "tails" behind each pulse approach one-another; this results in the system returning to the $u = 0$ state—the pulses annihilate (see Fig. 4). By adding two-point connections we introduce a mechanism for persistent self-sustaining activity; as in Roxin et al.'s discrete neuron model a connection can act as a shortcut from point x' to x. If a pulse reaches x' and the connection to x is strong enough to raise the activity at x above threshold, then two new oppositely travelling pulses will be created. By a "strong enough connection", here we mean that $w(x, x')$ is sufficiently large in this vicinity, which depends on parameters A and N, and the positioning of the peaks $\{x_n, x'_n\}$. Figure 5 shows how this self production of new pulses can lead to persistent activity in a particular realisation of the system; panel (a) shows a schematic diagram of the connections, (b) the integrated connection $W(x)$ (Eq. 8), and (c) a colour plot of activity changing in time. Panel (d) shows a snapshot

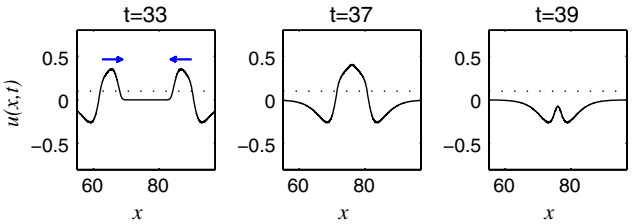

Fig. 4 *Plots* showing how two oppositely travelling pulses annihilate upon meeting. The *arrows* in the *leftmost panel* show the direction of motion of each pulse

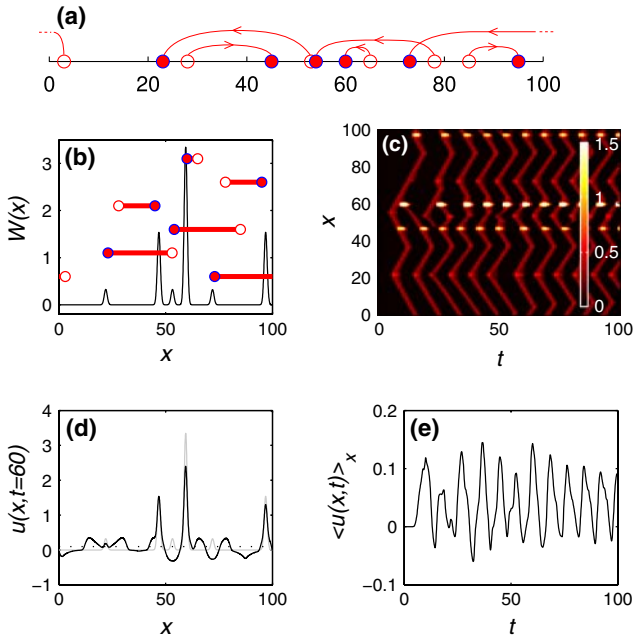

Fig. 5 *Plots* showing the connections and resulting activity (following injection of pulses into an initially quiescent system) of a particular realisation of the connections; each panel represents the same system, and the same region of space and time. For this example with $N = 6$ we observe self-sustained *non-local* persistent activity. **a** Schematic diagram showing the positions of the two-point connections. *Open circles* represent the start point of the connection and *filled circles* the end point. **b** Plot of the integrated connection $W(x)$, with *lines* showing the locations and directions of the two-point connections. Again *open* and *filled circles* represent the start and end point of the connections; the vertical position is arbitrary. We note that the end points of the connections give rise to "bumps" in $W(x)$. The length of the *arrow* represents the range of the connection, and we see from $W(x)$ that due to the inhomogeneous envelope $w_l(y)$, the shorter the *arrow*, the stronger the connection. **c** Colour plot showing the time evolution of the activity $u(x, t)$. **d** The *black line* shows a snapshot of $u(x, t)$ at $t = 60$, the *grey line* shows $W(x)$ and the *dotted line* is $u = \theta$. **e** Plot showing how the spatial average of the activity varies with time

of $u(x,t)$, and (e) shows how in a macroscopic measurement (in this case the spatial average of u), this manifests as persistent fluctuations of activity.

As well as this type of persistent activity (which is the analogue of the behaviour seen in Roxin et al. 2004), we observe a second type of persistent behaviour which was observed in the previous work (Brackley and Turner 2009). As we noted in the previous section, due to the inhomogeneous connections there are regions where $W(x) \geq \theta$, where locally an upper steady state exists. If this region is excited into the upper steady state, fronts will be produced at the edges of the region; as is detailed in Brackley and Turner (2009), due to the non-linear feedback these fronts periodically oscillate back and fourth about the boundary where $W(x) = \theta$. If a region where $W(x) \geq \theta$ is large enough that the oscillating fronts at each side of the region do not meet, the oscillation will persist, leading to a "breathing bump" of activity;[3] if the bump in $W(x)$ is too small, the fronts will meet and $u \to 0$. Since for the parameters chosen here ($g = 1$ and $\theta = 0.1$) travelling pulses are stable, the fluctuating fronts act as pulse emitters. Figure 6 shows this behaviour in a system with the same parameter set as in Fig. 5 but a different realisation of the connections. In order to be clear in describing these two very different types of behaviour we use the terms *non-local* persistent fluctuations and *breathing bump* persistent fluctuations referring to the phenomena seen in Figs. 5 and 6, respectively.

In order to glean insight into the effect of different parameters on system behaviour, we must examine many realisations of the connections. Below we find the probability of persistent fluctuations by looking at the proportion of realisations in which it is seen. Although in Figs. 5 and 6 we can clearly identify two different modes of fluctuation, we note that without detailed inspection of the dynamics we cannot tell the difference between them (e.g. from a macroscopic measurement such as $\langle u(x,t)\rangle_t$). Indeed one would expect a large system to have regions where *non-local* connections can provide persistent activity and regions with *breathing bumps*; thus for the majority of the following work we do not distinguish between these behaviours. However, we are able to distinguish between behaviour which depends on the type of initial conditions used to excite the system. If we inject a pulse into a system initially in the $u(x) = 0$ state, then both of the modes of persistent activity are excited. An alternative initial condition would be to set $u(x)$ equal to some constant greater than θ for all x; since there are no pulses, the system in Fig. 5 would not be excited into the fluctuating state, and after some transient would move to the $u(x) = 0$ steady state. The system in Fig. 6 on the other hand

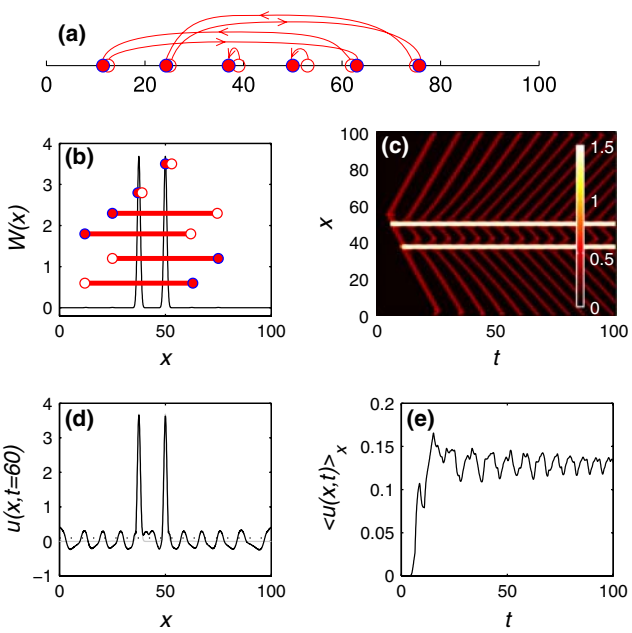

Fig. 6 *Plots* showing the connections and resulting activity of a particular realisation of the connections; each panel represents the same system, and the same region of space and time. For this example with $N = 6$ we observe *breathing bump* persistent fluctuations. **a** Schematic diagram showing the positions of the two-point connections. *Open circles* represent the start point of the connection and *filled circles* the end point. **b** Plot of the integrated connection $W(x)$, with lines showing the locations and directions of the two-point connections. Again *open* and *filled circles* represent the start and end point of the connections; the vertical position is arbitrary. **c** *Colour plot* showing the time evolution of the activity $u(x,t)$. **d** *The black line* shows a snapshot of $u(x,t)$ at $t = 60$, the *grey line* shows $W(x)$ and the dotted line is $u = \theta$. **e** *Plot* showing how the spatial average of the activity varies with time

would move into the fluctuating state since in has "bumps" in $W(x)$ large enough to lead to *breathing bumps* of activity and these *would* be excited. In conclusion, using a uniform initial condition (without injecting a pulse) can *only* excite a system containing breathing bumps to the fluctuating state.[4]

5 The probability of fluctuating states

We have seen that with certain choices of parameters our system can exist in either a quiet state or a fluctuating state, and by application of a transient input we can switch between the two. Such behaviour can be seen in working memory tasks; for example Wang (2001) reviews work where cells in primate cortex are seen to move in into a high-firing rate state for the duration of the delay period of a stimulus-delay-response task. Here we have shown that such behaviour can

[3] We note that this breathing bump exists via a different mechanism than reported in models with linear feedback (Coombes and Owen 2005; Bressloff et al. 2003).

[4] We note that once breathing bumps are produced they will emit travelling pulses which will spread throughout the system.

not only be seen in models on scales of IF cell networks (Roxin et al. 2004), but also in models at the population level. The two types of persistent behaviour described above both manifest as fluctuations when we look at a system wide (i.e. spatial average) level; this could be linked to mesoscopic scale measurements such as local field potentials (Wu et al. 1999).

Since we study stochastic connection functions, we cannot say defiantly whether a system with certain parameters will be able to support the fluctuating state, so in this section we study the *probability* that a particular realisation of the connections can exhibit persistent fluctuations P_{fluct} and how this varies with the quantity Nl/L. In all results below we look at 300 realisations of the connections, taking the proportion which exhibit fluctuations as the probability. Since examining $u(x,t)$ for all x and t would be both time consuming and computationally expensive, we instead retain only the time series of the spatial average of the activity $\langle u(x,t)\rangle_x$. After discarding data from the first 100 time units of any simulation run to account for transient behaviour, we find the variance of the time series; if this is greater than 10^{-4} activity units we class the system as exhibiting persistent fluctuations. We measure P_{fluct} by initialising the system such that $u = 0$ for all x, and injecting travelling pulses by introducing a localised transient input. The value of u will increase at the site of the input, and upon reaching threshold, two oppositely travelling pulses will be produced. We choose a square shaped input with height 0.2 and width 1 which lasts for a duration of 7 time units (this choice is arbitrary—the only conditions for generation of two pulses is that the input is symmetric about its centre, and lasts sufficiently long that the activity reaches threshold). As discussed above, by using a different initial condition of $u(x, t = 0) > \theta$, we can count the number of systems in which *breathing bumps* are possible. We denote this P_{breathe}.[5] Figure 7 shows P_{fluct} and P_{breathe} as functions of Nl/L for a system with $L = 100, l = 20$ and $A = 0.1$. In order to understand the shape of these curves we first consider the requirements for each type of persistent activity.

Firstly non-local fluctuations; in order that a pulse travelling over the start point of a connection produces new pulses at the end point, the connection must be strong enough to increase activity above threshold. That is, $W(x)$ must be greater than θ at the end point. The height of a "bump" in $W(x)$ (due to a single peak in w_A, e.g.) is determined by the height of peaks $(1/N)$ and the parameter A, as well as the normalisation $\mathcal{N} = L^2/d^2 l\pi^{3/2}$. We must also consider pulse annihilation which is due to the tail of depressed

[5] In summary P_{fluct} gives the probability that a system can exhibit persistent fluctuations. P_{breathe} counts *only* systems which can support a breathing bump.

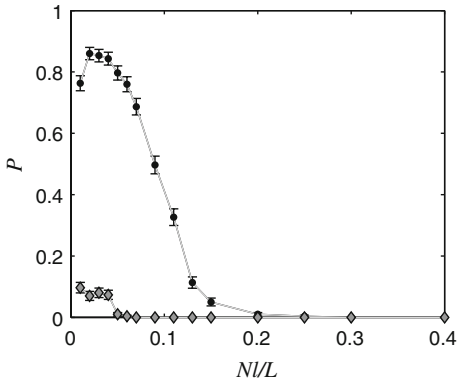

Fig. 7 *Plot* showing the probability that a particular realisation of the connections can support persistent fluctuations P_{fluct} as a function of Nl/L (points). Also shown (*diamonds*) is the probability that a realisation supports *breathing bump* fluctuations P_{breathe}. These results are based on a sample of 300 realisations. The *error bars* (shown here and in subsequent plots where they are larger than points) show the standard deviation of a binomial distribution. The points (here and in subsequent plots) are connected by linear interpolation as a guide for the eye

activity in the wake of the pulse (see Figs. 3, 4); this region cannot recover quickly enough to allow a second oppositely travelling pulse to propagate through it. If the start and end points of a heterogeneous connection are too close together, the two new pulses and the original pulse will annihilate each other. As described in the previous section *breathing bump* fluctuations require regions where $W(x) \geq \theta$ to have significant spatial extent (Brackley and Turner 2009).

Returning to the shape of curves in Fig. 7, we expect, at large N, the height of the peaks in w_A will be too small to allow either type of persistent activity. In this limit $W(x) \approx A$, and so $W(x)$ does not cut through threshold any where; the activity will reside in a steady state (whether one or two steady states exist depends on A). We see that *breathing bump* fluctuations only occur for Nl/L less than ~ 0.05, but *non-local* fluctuations still occur in approximately half of all realisations for $Nl/L \sim 0.1$. As Nl/L decreases P_{fluct} increases; as the number of connection decreases there is less chance of many pulses annihilating each other. The shape of the curve in the region corresponds to the sigmoid shape of the curves shown in Roxin et al. (2004) (where $1 - P_{\text{fluct}}$ is plotted).

When Nl/L is small there is a low probability that a peak in w_A will be placed within l of the $x = x'$ line on the x, x' plane, so we expect P_{fluct} to decrease again as $Nl/L \to 0$. Hence we see a peak in P_{fluct}. We note that P_{fluct} never reaches 1; this is because again there is a non-zero probability that all the peaks in w_A are placed further than a distance l away from the $x = x'$ line, and peaks placed too close to this line can lead to pulse annihilation. These features are a result of our quasi-random placing of peaks over the whole x, x' plane, and the Gaussian form of w_l.

6 The role of connection strength A, maximum range l and system size L

Figure 8 shows plots of $P_{\text{fluct}}(Nl/L)$ for several different values of A close to threshold $\theta = 0.1$. We see the trend that, as we increase A, there is greater probability of fluctuations. The peaks in w_A have a height $A\mathcal{N}/N$, so increasing this means that there is more chance of having connections which lead to new pulses being generated and hence fluctuating activity. For $A = 0.2$ we see a non-zero probability of fluctuations at much higher Nl/L than for smaller A. In the large N limit $W(x) \to A$, so in this case where $A > \theta$, we expect the activity to sit in the upper steady state; if, however, there is even the smallest region where $W(x) < \theta$ and there is no upper steady state, then this will not be possible and the remaining options for the system are fluctuations, or collapse to the $u = 0$ steady state. At small Nl/L there seems to be no dependence on A; here the peaks in w_A are large enough that small variation in A does not change whether $W(x) \geq \theta$ at the end points of connections.

Figure 9a shows plots of $P_{\text{fluct}}(Nl/L)$ for several different values of l, the maximum range of long distance connections. We see that, as we increase l for fixed number of connections, P_{fluct} increases. For fixed Nl/L if we increase l we are effectively spreading the same number of peaks over a larger area on the x, x' plane. We noted in 5 that *non-local* fluctuations require the start and end points of connections to be sufficiently separated; spreading the same number of points over a larger area allows start and end points to be more separated, so we expect the probability of *non-local* fluctuations to increase. Figure 9b shows that if we look only at *breathing bump* fluctuations, the opposite trend is seen: P_{breathe} decreases with l. This again makes sense, since as we decrease l for fixed Nl/L we are placing the same number of peaks in a smaller area on the x, x' plane and increasing

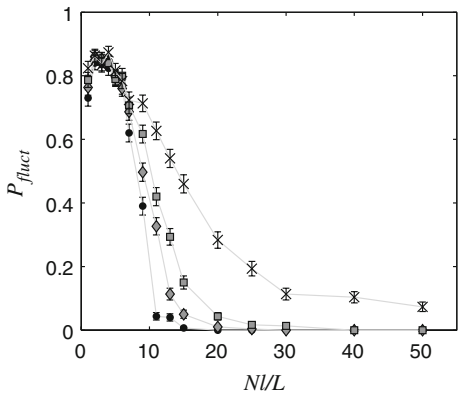

Fig. 8 *Plot* showing the probability that a realisation supports fluctuations as a function of Nl/L for different A. *Points*, *diamonds*, *squares* and *crosses* show $A = 0.08$, $A = 0.1$, $A = 0.12$ and $A = 0.2$, respectively. The other parameters are $\theta = 0.1$, $l = 20$ and $L = 100$

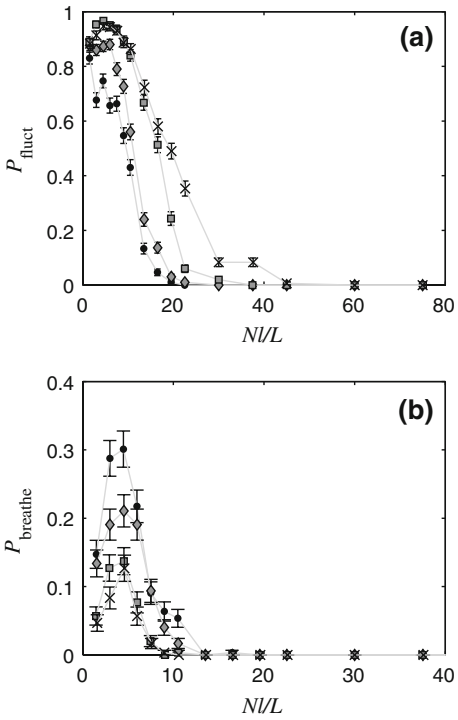

Fig. 9 **a** *Plot* showing the probability that a realisation supports fluctuations as a function of Nl/L for different envelope width l. *Points*, *diamonds*, *squares* and *crosses* show $l = 7$, $l = 10$, $l = 20$ and $l = 30$, respectively. The other parameters are $A = 0.1$ and $L = 150$. **b** *Plot* showing data from the same systems but with initial conditions which only allow *breathing bump* fluctuations to occur

the liklihood of peaks overlapping, which can give rise to significantly extended regions where $W(x) > \theta$. Malach et al. (1994) finds that patches are located within several times the local connection width, which corresponds to small l in our model, where we find that there is a significant probability of observing fluctuations.

In Fig. 10 we examine the effect of changing the system size L. In this case we do not look at the probability of fluctuations at different numbers of two-point connections Nl/L, but rather at the density of connections N/L^2. As we expect, both P_{fluct} and P_{breathe} increase with system size for given N/L^2. If the probability of fluctuations *not* occurring in a system of size L is $1 - P(L)$, then we expect that in a system of length $2L$ the probability of fluctuations not occurring will be $[1 - P(L)]^2$. Following this argument, given a system size L, a system of size βL has a probability of fluctuation of $P(\beta L) = 1 - [1 - P(L)]^{\beta}$. By using the largest system we simulated ($L = 200$) as a reference we can construct an equation for P_{fluct} for any value of L and connection density N/L^2

$$P_{\text{fluct}}(L) = 1 - [1 - P_{200}(N/L^2)]^{L/200}, \tag{12}$$

where $P_{200} = P_{\text{fluct}}|_{L=200}$, and is found at any value of N/L^2 by fitting a smoothing cubic spline to the $L = 200$ data shown

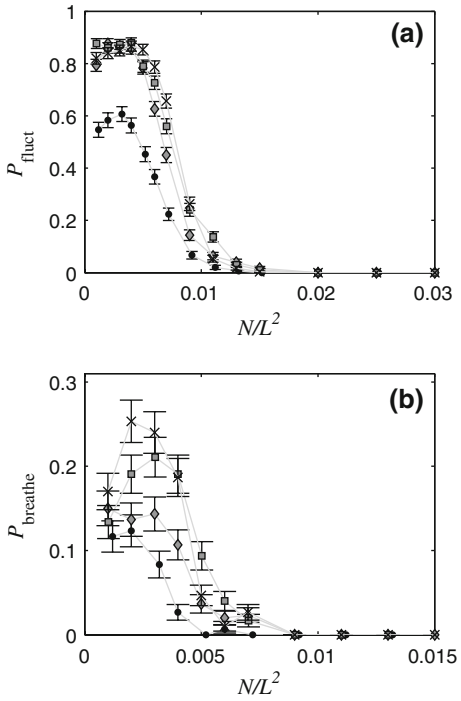

Fig. 10 **a** *Plot* showing the probability that a realisation supports fluctuations as a function of connection density N/L^2 for different system sizes. *Points*, *diamonds*, *squares* and *crosses* show $L = 50$, $L = 100$, $L = 150$, and $L = 200$, respectively. The other parameters are $A = 0.1$ and $l = 10$. **b** *Plot* shows the probability of *breathing bump* fluctuations for the same systems

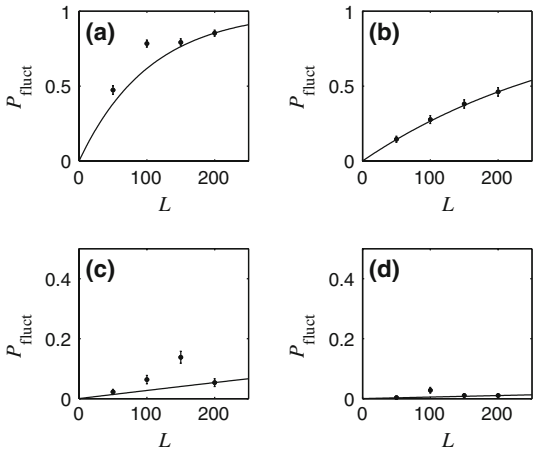

Fig. 11 *Plots* showing P_{fluct} as a function of system size L at different connection densities N/L^2. *Plots* show **a** $N/L^2 = 0.005$, **b** $N/L^2 = 0.008$, **c** $N/L^2 = 0.011$, and **d** $N/L^2 = 0.014$. The *solid line* shows Eq. (12). *Error bars* are shown where they are larger than the points

in Fig. 10a. This represents an approximation to the *universal* probability that a system of size L fluctuates.

In Fig. 11 we plot probability against L at different densities; the error bars shows the standard deviation in the probability. Solid lines show Eq. (12). Figure 12 shows a 3D surface plot P_{fluct} as a function of both L and N/L^2 from

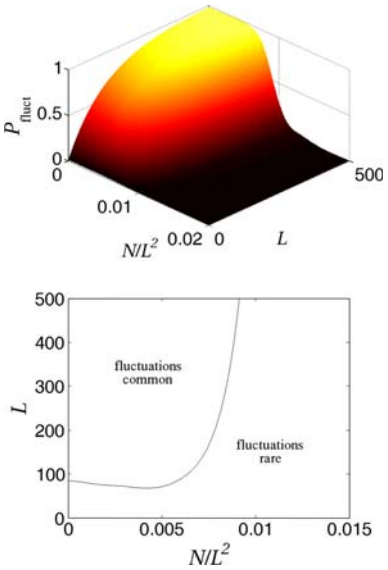

Fig. 12 *Top* Plot showing P_{fluct} as a function of system size L and connection density N/L^2 as given by Eq. (12). Values of $P_{200}(N/L^2)$ are found from data shown in Fig. 10a using smoothing cubic splines. *Bottom* contour plot of the same function showing a single contour at $P_{\text{fluct}} = 0.5$

Eq. (12). Also shown is a contour plot showing $P_{\text{fluct}} = 0.5$ in the L, N/L^2 plane; this can be thought of as the boundary between the region of parameter space where a system is likely to exhibit fluctuations, and the region where it is unlikely that a system can support fluctuations.

As we would expect, for stochastically placed connections, the larger the system, the greater the liklihood that there will be an arrangement of connections which leads to fluctuations. Experimentally, fluctuations have been seen in even small isolated pieces of tissue; this could be an indication of non-random structure in the connectivity of real tissue. We note also that in this regime of travelling pulses, even if fluctuations originate only at one point in a large system, these will spread to cover the whole system.

We have also examined how the frequency of fluctuations is effected by the density of connections and the length l. We take the fast Fourier transform of the time series $\langle u(x,t)\rangle_x$ for realisations where persistent fluctuations take place, and examine the frequency with the largest amplitude. As Nl/L is increased there is a decrease in frequency, but no effect (to within standard error) when varying l at constant Nl/L (data not shown). We expect this since, for *non-local* persistent fluctuations, frequencies are determined by the distance over which pulses travel between re-injection of activity to produce new pulses. Using suitable order of magnitude estimates for parameters ($\tau_u = 10$ ms, see McCormick et al. (1985)) the frequencies measured were within the range 8–15Hz; although this model is mainly qualitative it is encouraging that these frequencies are in the range seen

experimentally in, for example local field potentials (Wu et al. 1999) or EEG (Nunez and Srinivason 2006).

7 Addressing further simplifications

As detailed in the introduction section, in order to reduce the number of free parameters in our model, in the above calculations we take $\tau_v = \tau_u$. We have performed several calculations using different values of τ_v. Figure 13 shows that as we increase τ_v (i.e. we slow down the response of the inhibitory population), the probability of fluctuations decreases. (This is true except at small Nl/L where we argue that the sample size is insufficient to get accurate statistics.) It can be shown (by following methods in Coombes (2005)) that in the homogeneous model, for a given τ_v there can be two travelling pulse solutions, one stable and one unstable. Figure 14 shows the two branches of solutions for the speed (c) and width (Δ) of the pulse as a function of τ_v. We see that in the stable branch, as τ_v increases, c remains constant whilst Δ increases. Larger width means a larger region of depressed activity in the wake of a travelling pulse; start and end points of connections need to be further apart to avoid annihilation, leading to decreased probability of persistent activity. In summary slower inhibition leads to wider pulses which reduces the liklihood of persistent fluctuations.

The other simplification we make is to take the width of the heterogeneous connection patches $d = 1$, despite the fact that evidence such as Fig. 1 suggests that long range patches would have a width less than that of the homogeneous connections. Since the local connections are present everywhere in our system, one might argue that features on length scales shorter than these would be averaged out. However, we also note that the normalisation of the inhomogeneous component of the connection function $\mathcal{N}$ contains a factor $1/d^2$; i.e. reducing the width of peaks in w_A will increase their height. Figure 15 shows results for $d = 0.5$ and $d = 1$; we see a similar difference between the two as we do when we increase the amplitude of the connection A (Fig. 8).

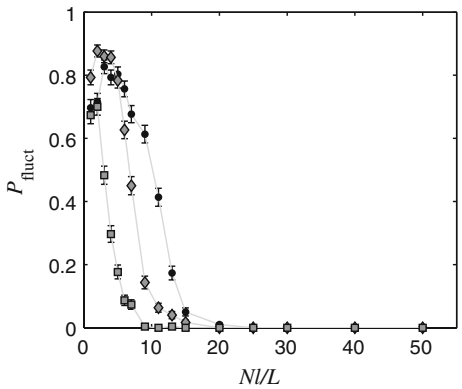

Fig. 13 *Plot* showing $P_{\rm fluct}$ as a function of Nl/L with $L = 100, l = 10$ and $A = 0.1$ for different values of the inhibitory population time constant τ_v. *Points*, *diamonds* and *squares* show $\tau_v = 0.5, \tau_v = 1$, and $\tau_v = 2$, respectively

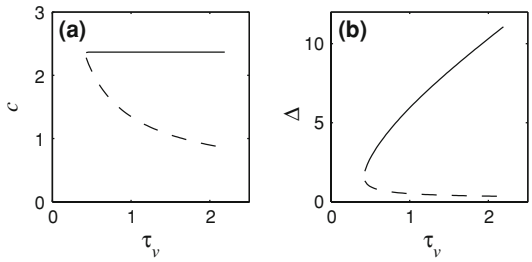

Fig. 14 *Plots* showing **a** the speed c, and **b** the width Δ, of travelling pulse solutions in a homogeneous system, as a function of τ_v with $g = 1$. Stable branches are *solid lines* and *unstable dashed*

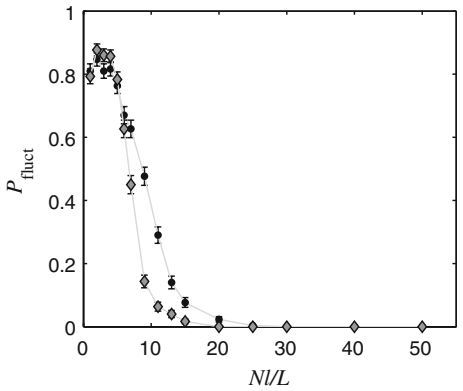

Fig. 15 *Plot* showing $P_{\rm fluct}$ as a function of Nl/L with $L = 100, l = 10$ and $A = 0.1$ for different values of the width of long range two-point connections d. *Points* and *diamonds* show $d = 0.5$ and $d = 1$, respectively

8 Conclusions

With this model we have shown that the well known solutions to homogeneous CNF models (travelling fronts and pulses) are robust to the addition of a small number of heterogeneous connections between points in the system. Our choice of inhomogeneous connections is motivated by previous work on networks of simple excitable integrate and fire neurons, and experimental evidence of "patchy" connectivity seen in visual cortex.

We have identified two new types of behaviour, which on a system scale manifest as persistent fluctuations of activity. The self sustained activity which occurs due to *non-local* connections is analogous to that seen in a small-world network of IF neurons (Roxin et al. 2004). Travelling pulses lead to the re-injection of activity at distantly connected points; as with the previous study the fact that two pulses annihilate (due to

"tails" of depressed activity) means there is a mechanism to switch between the fluctuating and quiet states.

The second mode of persistent fluctuation arises if a region of the system receives sufficient incoming connections that there exists locally an upper steady state. As we have seen previously in similar models (Brackley and Turner 2009), if such regions are sufficiently large, activity can remain in the upper state locally, and fluctuations will be seen at the boundaries. In the work presented here we choose a regime where travelling pulses are stable, meaning pulses are emitted from the fluctuating boundaries. This is in contrast to our previous paper (Brackley and Turner 2009) where we look at breathing bump type persistent activity in a model with a different form of inhomogeneous connections, in a regime which does not support pulses. There, instead of introducing inhomogeneity by adding two-point connections, a continuous inhomogeneous term with a power law envelope was added; coherence of fluctuations across 1D and 2D systems was investigated as a function of connection range.

In summary, in this study, we find that as we increase the number of two-point connections the probability of persistent fluctuations decreases. The reason for this is twofold; firstly too many connections can lead to (almost) the entire system being excited by a single pulse within a time too short for the activity to recover to resting. Secondly our choice of $1/N$ normalisation of two-point connections means as N gets large the incoming connections $W(x)$ becomes constant in space. We also see that P_{fluct} is extensive in system size.

For reasons of computational efficiency the work here focuses on a 1D system. This might be applicable to, for example thin channels of highly connected neurons (e.g. the infrapyramidal bundle), or could represent functional space rather than real space. The extension to 2D would a low for a much more realistic representation of cortical tissue. We have randomly positioned our connections, whereas a 2D model would allow some structure to be introduced, e.g. increased liklihood of connection between regions of similar orientation preference. It would be interesting to look at spatial correlations in the activity patterns, and see to what degree these reflect the structure of the connections, although we acknowledge that the development of more efficient methods for numerically evaluating integrals is a computational challenge.

As discussed in the introduction section, a feature *not* present in the current model (as it is neither in the classic paper of Amari (1977)) is finite axonal propagation velocity (in contrast to the work by the Jirsa group Jirsa and Kelso 2000; Qubbaj and Jirsa 2007). It would be an interesting future study to see how including this might effect our results, and is of particular concern for systems with long ranging connections (large l in the present context) where finite velocity will become important. For example one might expect that a delay in activation of a region via a long range connection will have important consequences for the annihilation of "daughter" pulses by a parent pulse if, for example the axonal propagation velocity is of similar magnitude as the pulse velocity. The current work could be used as a guide to identify which phenomena are due to finite action potential velocity and which are due to patchy connections. Also Qubbaj and Jirsa (2007) and others (Hutt et al. 2003; Venkov et al. 2007; Hutt and Atay 2005) study a parameter regime where the uniform steady state becomes unstable (via a Turing or Hopf instability) and spatio-temporal patterns are seen, whereas we focus on a regime where the system can be switched from fluctuating to quiet and back again. An interesting extension to the present model and those works mentioned above would be to examine the effect of multiple "patchy" connections on spatio-temporal pattern formation of this type.

Acknowledgments We gratefully acknowledge stimulating discussion with Magnus Richardson and George Rowlands. We also acknowledge the Centre for Scientific Computing at the University of Warwick for use of desktop and HPC systems.

Appendix A: Numerical methods

The differential equations (1) are solved numerically by discretising a finite system of length L in space and time with fixed grid size and time step a and δt, respectively. We thus have a set of L/a coupled differential equations which we solve using a fourth order Runge–Kutta routine based on those in Press et al. (1992). We use periodic boundary conditions.

The integral on left hand side of the equation for u can be separated into two terms

$$\int_{x-\frac{L}{2}}^{x+\frac{L}{2}} w_H(|x-x'|)\, f(u(x',t))\mathrm{d}x' + \int_{x-\frac{L}{2}}^{x+\frac{L}{2}} A w_I(|x-x'|) w_A(x,x')\, f(u(x',t))\mathrm{d}x', \qquad (13)$$

where we have chosen the limits to take into account the periodicity of the system. We note that the first integral is of convolution form, and can therefore be evaluated using fast Fourier transform routines (Frigo and Johnson 2005); this method is very computationally efficient (and intrinsically assumes periodic boundaries). The second integral is much more computationally expensive to evaluate. Although there are a wealth of well known standard methods for evaluating integrals most are unsuitable for this problem since the integrand contains the discontinuous function $f(u)$ and u is only known at points on a regular grid. We resort to a simple

application of the trapezium rule (again see Press et al. 1992). This method is very time consuming, and we have to evaluate the integral four times per time step (due to fourth order Runge–Kutta). Since the integral is over the Gaussian function w_l which has characteristic width l, we improve performance by truncating this function when $|x-x'| = l\sqrt{\ln(500)}$.

As described in Sect. 2, to generate $w_A(x, x')$ we place peaks at maximally self avoiding positions using a sequence of quasi-random numbers. These are generated using a Sobol sequence (Press et al. 1992; Sobol' 1967). This generates numbers between 0 and 1 in their binary representation by changing each bit at different rates as you step though the sequence. We use a 2D Sobol sequence; when points are added to the plane they fill in gaps between existing points; the first N peaks are maximally avoiding, as are the next N. We can generate different realisations of the system by taking successive groups of points from the sequence; the limit on the number of points is the length of the binary "word" representing the numbers. Using a sequence like this reduces the chance of several peaks sitting on top of each other in clusters (although admittedly it may also introduce other features).

In all work presented here we use $a = 0.05$ and $\tau = 0.1$. These values were chosen as a compromise between computational runtime and accuracy; we performed several calculations using smaller values (not shown) and found no significant change in results. System sizes of $L \sim 100$ were used as a compromise between having the largest system possible and computational runtime. We also note that simulating a 2D system with these methods is computationally infeasible, both in respect of simulation runtime, and data storage, for example of the values of the function $w_A(x, x')$ at $(L/a)^2$ grid points.

References

Amari SI (1977) Dynamics of pattern formation in lateral-inhibition type neural fields. Biol Cybern 27:77–87

Bao W, Wu JY (2003) Propagating wave and irregular dynamics: Spatiotemporal patterns of cholinergic theta oscillations in neocortex in vitro. J Neurophys 90:333–341

Brackley CA, Turner MS (2007) Random fluctuations of the firing rate function in a continuum neural field model. Phys Rev E 75:041,913

Brackley CA, Turner MS (2009) Persistent fluctuations of activity in undriven continuum neural field models with power-law connections. Phys Rev E 79:011918

Bressloff PC (1996) New mechanism for neural pattern formation. Phys Rev Lett 76(24):4644–4647

Bressloff PC (2001) Traveling fronts and wave propagation failure in an inhomogeneous neural network. Phys D Nonlinear Phenom 155(1–2):83–100

Bressloff PC (2003) Spatially periodic modulation of cortical patterns by long-range horizontal connections. Phys D Nonlinear Phenom 185(3–4):131–157

Bressloff PC, Folias SE, Prat A, Li YX (2003) Oscillatory waves in inhomogeneous neural media. Phys Rev Lett 91(17):178,101

Brunel N (2000) Dynamics of sparsely connected networks of excitatory and inhibitory spiking neurons. J Comput Neurosci 8:183–208

Buzás P, Eysel UT, Adorján P, Kisvárday ZF (2001) Axonal topography of cortical basket cells in relation to orientation, dierection, and ocular dominance maps. J Comp Neurol 437:259–285

Coombes S (2005) Waves, bumps, and patterns in neural field theories. Biol Cybern 93:91–108

Coombes S, Owen MR (2005) Bumps, breathers, and waves in a neural network with spike frequency adaption. Phys Rev Lett 94: 148,102

Coombes S, Lord GJ, Owen MR (2003) Waves and bumps in neuronal networks with axo-dendritic synaptic interactions. Phys D Nonlinear Phenom 178:219–241

Cossart R, Aronov D, Yuste R (2003) Attractor dynamics of network up states in the neocortex. Nature 423:283–288

Ermentrout GB, Cowan JD (1979) A mathematical theory of visual hallucination patterns. Biol Cybern 34:137–150

Ermentrout GB, McLeod JB (1993) Existence and uniqueness of travelling waves for a neural network. Proc Sect A Math R Soc Edinb 123:461–478

Frigo M, Johnson SG (2005) The design and implementation of fftw3. Proc IEEE 93:216–231

Hellwig B (2000) A quantitative analysis of the local connectivity between pyramidal neurons in layers 2/3 of the rat visual cortex. Biol Cybern 82:111–121

Hopfield JJ (1982) Neural networks and physical systems with emergent collective computational abilities. Proc Natl Acad Sci USA 79(8):2554–2558

Hutt A, Atay FM (2005) Analysis of nonlocal neural fields for both general and gamma-distributed connectivities. Phys D Nonlinear Phenom 203:30–54

Hutt A, Wennekers T, Bestehorn M (2003) Pattern formation in intracortical neuronal fields. Netw Comput Neural Syst 14:351–368

Jirsa VK (2004) Connectivity and dynamics of neural information processing. Neuroinformatics 2:183–204

Jirsa VK, Kelso JAS (2000) Spatiotemporal pattern formation in neural systems with heterogeneous connection topologies. Phys Rev E 62(6):8462–8465

Malach R, Tootell RBH, Malonek D (1994) Relationship bewteen orientation domains, cytochrome oxidase stripes, and intrinsic horizontal connections in squirrel monkey area v2. Cereb Cortex 4(2):151–165

McCormick DA, Connors BW, Lighthall JW, Prince DA (1985) Comparative electrophysiology of pyramidal and sparsely spiny stellate neurons of the neocortex. J Neurophysiol 54(4):782–806

Nunez PL, Srinivason R (2006) Electric fields of the Brain—the neurophysics of EEG, 2nd edn. Oxford University Press, Oxford

Pinto DJ, Ermentrout GB (2001) Spatially structured activity in synaptically coupled neuronal networks: I. travelling fronts and pulses. SIAM J Appl Math 62:206–225

Press H, Teukolsky SA, Vetterling WT, Flannery BP (1992) Numerical recipes in fortran, 2nd edn. Cambridge University Press, Cambridge

Qubbaj MR, Jirsa VK (2007) Neural field dynamics with heterogeneous connection topology. Phys Rev Lett 98(23):238,102

Robinson PA, Rennie CJ, Rowe DL (2002) Dynamics of large-scale brain activity in normal arousal states and epileptic seizures. Phys Rev E 65(4):041,924

Roxin A, Riecke H, Solla SA (2004) Self-sustained activity in a small-world network of excitable neurons. Phys Rev Lett 92: 198,101

Segev R, Benveniste M, Hulata E, Cohen N, Palevski A, Kapon E, Shapira Y, Ben-Jacob E (2002) Long term behavior of lithographically prepared in vitro neuronal networks. Phys Rev Lett 88:118,102

Sobol' IM (1967) The distribution of points in a cube and the accurate evaluation of integrals. USSR Comput Math Math Phys 7(4):86–112

Venkov N, Coombes S, Matthews P (2007) Dynamic instabilities in scalar neural field equations with space-dependent delays. Phys D Nonlinear Phenom 232:1–15

Wang XJ (2001) Synaptic reverberation underlying mnemonic persistent activity. TRENDS Neurosci 24:455–463

Wilson HR, Cowan JD (1972) Excitatory and inhibitory interactions in localized populations of model neurons. Biophys J 12:1–23

Wu JY, Guan L, Tsau Y (1999) Propagating activation during oscillations and evoked responses in neocortical slices. J Neurosci 19:5005–5015